AIAA JOURNAL
Vol. 41, No. 10, October 2003

Technical Note

TECHNICAL NOTES are short manuscripts describing new developments or important results of a preliminary nature. These Notes cannot exceed six manuscript pages and three figures; a page of text may be substituted for a figure and vice versa. After informal review by the editors, they may be published within a few months of the date of receipt. Style requirements are the same as for regular contributions (see inside back cover).

Sensitivity to the Smagorinsky Constant in Turbulent Jet Simulations

Ali Uzun,* Gregory A. Blaisdell,†
and Anastasios S. Lyrintzis‡
Purdue University, West Lafayette, Indiana 47907

Introduction

THE turbulent jet noise problem still remains one of the most complicated and difficult problems in aeroacoustics. There is a substantial need for improved jet noise prediction methodologies and design processes for aircraft engines with low jet noise emissions. With the recent improvements in the processing speed of computers, the application of direct numerical simulation (DNS)[1] and large eddy simulation (LES)[2–6] to jet noise prediction methodologies is becoming more feasible. However, due to the wide range of length scales and timescales present in turbulent flows, DNS is still restricted to low-Reynolds-number flows in relatively simple geometries. LES, with lower computational cost, is an attractive alternative to DNS. Because noise generation is an inherently unsteady process, LES will probably be the only way, other than DNS, to obtain the necessary time-accurate unsteady data at an affordable cost in the foreseeable future. In general, the LES results for turbulent jets in the literature to date are encouraging and show the potential promise of LES application to jet noise prediction.

In an LES, the flowfield is decomposed into a large-scale or resolved-scale component $\bar{f}$ and a small-scale or subgrid-scale component f', i.e., $f = \bar{f} + f'$. The large-scale component is obtained by filtering the entire domain using a grid filter function G with filter width Δ as follows:

$$\bar{f}(\boldsymbol{x}) = \int_V G(\boldsymbol{x}, \boldsymbol{x}', \Delta) f(\boldsymbol{x}') \, \mathrm{d}\boldsymbol{x}' \tag{1}$$

The filtering operation removes the small-scale or the subgrid-scale turbulence from the Navier–Stokes equations. The resulting governing equations are then solved directly for the large-scale turbulent motions while the effect of the subgrid scales is computed using a subgrid-scale model, such as the classical Smagorinsky model[7] or the more sophisticated dynamic model proposed by Germano et al.[8]

The Smagorinsky model is the most widely used subgrid-scale model due to its simplicity. It requires only a model coefficient to be specified a priori to the simulation. In this study, we will discuss the model's sensitivity by applying it to the LES of turbulent jets and analyzing the results of two simulations obtained with slightly direrent values of the model constant. The Smagorinsky model is known to be sensitive to values of the model constant; however, our simulations show explicitly how strongly the mean flow properties of the jets are sensitive to the value of the model constant. More detailed results can be found in Ref. 5.

Received 10 December 2002; revision received 12 June 2003; accepted for publication 12 June 2003.

*Graduate Research Assistant, School of Aeronautics and Astronautics. Member AIAA.
†Associate Professor, School of Aeronautics and Astronautics. Senior Member AIAA.
‡Professor, School of Aeronautics and Astronautics. Associate Fellow AIAA.

Governing Equations

The governing equations for LES are obtained by applying a spatial filter to the Navier–Stokes equations in order to remove the small scales. The effect of the subgrid scales is computed using the classical Smagorinsky subgrid-scale model[7] together with the compressibility correction formulated by Erlebacher et al.[9] Because we are dealing with compressible jet flows, the Favre-filtered unsteady, compressible, nondimensionalized Navier–Stokes equations formulated in curvilinear coordinates[10] are solved in this study using the numerical methods described in the next section.

In our implementation, the subgrid-scale stress tensor is modeled as follows:

$$\tau_{ij} = -2C\bar{\rho}\Delta^2\tilde{S}_M\left(\tilde{S}_{ij} - \tfrac{1}{3}\tilde{S}_{kk}\delta_{ij}\right) + \tfrac{2}{3}C_I\bar{\rho}\Delta^2\tilde{S}_M^2\delta_{ij} \tag{2}$$

where

$$\tilde{S}_{ij} = \frac{1}{2}\left(\frac{\partial\tilde{u}_j}{\partial x_i} + \frac{\partial\tilde{u}_i}{\partial x_j}\right), \qquad \tilde{S}_M = (2\tilde{S}_{ij}\tilde{S}_{ij})^{\frac{1}{2}} \tag{3}$$

C, C_I are the model coefficients, and Δ is the filter width or the eddy viscosity length scale.

Numerical Methods

We first transform a given nonuniformly spaced curvilinear computational grid in physical space to a uniform grid in computational space and solve the discretized governing equations on the uniform grid. To compute the spatial derivatives at interior grid points away from the boundaries, we employ the nondissipative, sixth-order compact scheme of Lele.[11] For the boundary points, we use the third-order, one-sided compact scheme, and for the points next to the boundaries, we use the fourth-order central compact scheme.

Spatial filtering can be used as a means of suppressing unwanted numerical instabilities that can arise from the boundary conditions, unresolved scales, and mesh nonuniformities. In our study, we considered the following sixth-order, tridiagonal filter used by Visbal and Gaitonde[12]:

$$\alpha_f\hat{f}_{i-1} + \hat{f}_i + \alpha_f\hat{f}_{i+1} = \sum_{n=0}^{3}\frac{a_n}{2}(f_{i+n} + f_{i-n}) \tag{4}$$

where

$$a_0 = 11/16 + 5\alpha_f/8, \qquad a_1 = 15/32 + 17\alpha_f/16$$
$$a_2 = -3/16 + 3\alpha_f/8, \qquad a_3 = 1/32 - \alpha_f/16 \tag{5}$$

The parameter α_f must satisfy the inequality $-0.5 < \alpha_f < 0.5$. A less dissipative filter is obtained with higher values of α_f within the given range. With $\alpha_f = 0.5$, there is no filtering effect.

The standard fourth-order explicit Runge–Kutta scheme is used for time advancement. We apply Tam and Dong's three-dimensional radiation and outflow boundary conditions (see Ref. 13) on the

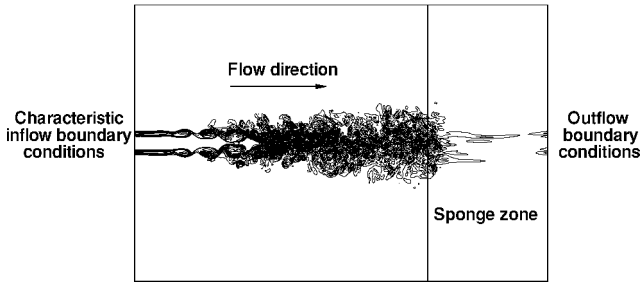

Fig. 1 Schematic of the boundary conditions.

boundaries of the computational domain as illustrated in Fig. 1. We additionally use the sponge zone method[13] in which grid stretching and artificial damping are applied to dissipate the vortices present in the flowfield before they hit the outflow boundary. This way, unwanted reflections from the outflow boundary are suppressed. The inflow boundary is responsible for both allowing outgoing acoustic waves to leave the domain as well as generating disturbances that trigger the growth of instabilities in the flowfield. For the inflow boundary conditions, we apply a procedure based on characteristics.[4] The forcing procedure that mimics the inlet turbulence is described next.

Results

We show results for a turbulent round jet at a Mach number of 0.9 and Reynolds number $Re_D = \rho_j U_j D_j/\mu_j = 3.6 \times 10^4$, where ρ_j, U_j, and μ_j are the jet centerline density, velocity, and viscosity at the nozzle exit, respectively, and D_j is the jet diameter. The ratio of the jet centerline density to the ambient density was chosen as 0.86. The stretched Cartesian grid used in this test case had $350 \times 128 \times 128$ points in the x, y, and z directions, respectively. Our domain extends to about $45r_o$ in the streamwise direction and from $-15r_o$ to $15r_o$ in the transverse y and z directions, where $r_o = D_j/2$ is the jet radius. The grid has almost 6 million grid points total. It should be noted here that the LES of Constantinescu and Lele[3] that produced good results for a Reynolds number 7.2×10^4 jet used a grid consisting of 3.9 million points. Their cylindrical domain extended $60r_o$ in the streamwise direction and $11r_o$ in the radial direction. Furthermore, the sponge layers of the grid used by Constantinescu and Lele[3] consisted of 20% of their total number of grid points, whereas our sponge layer consisted of only 8.5% of the total number of grid points. After doing a careful comparison of our grid with the grid used by Constantinescu and Lele,[3] it was determined that the grid resolution in our test case is more than enough for a Reynolds number 3.6×10^4 jet. The inflow velocity profile in our simulation is specified as a hyperbolic tangent top-hat profile. It should be noted here that because a Cartesian grid is used, the shear layer resolution is not the same at all azimuthal locations. However, the average number of grid points in the initial jet shear layer is about eight, which has been found to be sufficient to accurately resolve the shear layer.

For the inflow forcing in this test case, we applied the same kind of forcing used by Constantinescu and Lele[3] in their LES calculations. In this forcing, time-harmonic fluctuations are imposed on the mean streamwise velocity on the inflow boundary as follows:

$$v_x(r) = \tfrac{1}{2}U_o\{1 - \tanh[b(r/r_o - r_o/r)]\}[1 + \alpha \sin(2\pi Srt)] \quad (6)$$

where the Strouhal number $Sr = 2r_o f/U_o$ is 0.9, r_o is the jet radius, U_o is the mean jet centerline velocity on the inflow boundary, f is the frequency of the perturbations, $b = 3.125$ is the shear layer thickness parameter, and the amplitude of the sinusoidal oscillations α is 0.005. Randomly generated perturbations are applied on the azimuthal velocity component using the following equation:

$$v'_\theta(r, \theta) = 0.025U_o\epsilon \exp\left[-3(1 - r/r_o)^2\right] \quad (7)$$

where ϵ is a random number between -0.5 and 0.5. The mean azimuthal velocity on the inflow boundary is zero. The exponential function in Eq. (7) localizes the perturbations within the shear layer region only.

We did two runs for this test case and looked at the effect of varying the Smagorinsky constant. The Smagorinsky constant was chosen as 0.018 and 0.019 in the first and second simulations, respectively. The compressibility correction constant C_I was set to 0.0066, the filtering parameter was chosen as $\alpha_f = 0.49$, and all other parameters were kept the same for both simulations. Using 128 processors on an IBM-SP computer, 3 days of computing time was needed for a full simulation. We also did a Kolmogorov length scale analysis and determined that our coarsest grid resolution for this Reynolds number was between 50 and 60 times the local Kolmogorov length scale.

We compare some of our mean flow results obtained in the two simulations with each other as well as with the experimental data of Hussein et al.[14] for an incompressible jet at $Re_D = 9.55 \times 10^4$ and that of Panchapakesan and Lumley[15] for an incompressible jet at $Re_D = 1.1 \times 10^4$. The convective Mach number of the jet flow at the $x = 25r_o$ downstream location is about 0.2 and gets smaller for locations farther downstream. Owing to these low Mach numbers in the far-downstream region of the jet, the compressibility effects can be assumed negligible. Therefore, it is safe to compare our profiles in the far-downstream region with incompressible experimental data.

Using the mean streamwise velocity data, we first looked at the streamwise variation of the inverse of the mean centerline velocity normalized by the jet inflow velocity. The potential core of the jet breaks up at around $x = 14r_o$ in both simulations. After transition to turbulence, we obtained a linear growth that is consistent with experimental observations. Half of the inverse of this line's slope is equal to the jet decay coefficient, which was found to be approximately 5.0 for the simulation with $C = 0.018$. Experimental values of the jet decay coefficient are in between 5.4 and 6.1. Our computed jet spreading rate in this simulation, on the other hand, was found to be 0.106. The jet spreading rate is the slope of the linear growth of the half-velocity radius in the fully turbulent region. The half-velocity radius is defined as the radial location where the mean streamwise velocity is half of the mean centerline streamwise velocity at that axial location. Experimental values for the jet spreading rate range from 0.086 to 0.096. So with $C = 0.018$, we see that our jet opens up more than experimental jets because it has a low decay coefficient and a high spreading rate.

In the second simulation, in which a slightly larger Smagorinsky constant, $C = 0.019$, was used, we got a jet decay coefficient of 5.76, which is well within the range of experimental observations. The jet decay coefficient obtained with $C = 0.018$ was 5.0, a bit smaller than the lower limit of experimental data. The reason for this difference is believed to be the fact that with a higher Smagorinsky model constant, the jet loses more of its energy into dissipation and does not have as much energy left to spread out. Furthermore, with an increasing jet decay coefficient, the jet spreading rate gets smaller. This is justified by the fact that a jet spreading rate of 0.106 is obtained with $C = 0.018$, whereas a value of 0.086 is obtained with $C = 0.019$. Hence, the jet decay coefficient as well as the jet spreading rate are directly affected by the Smagorinsky model constant. For a 5.56% increase in the model constant, the jet decay coefficient increases by 15.20%, whereas the jet spreading rate decreases by 18.87%.

Figure 2 shows the computed Reynolds shear stress σ_{rx} profiles from the two simulations and compares them with the experimental data. The normalized Reynolds shear stress in cylindrical coordinates is defined as $\sigma_{rx} = \overline{v'_r v'_x}/U_c^2$, where v'_x and v'_r are the axial and radial components of the fluctuating velocity, respectively, U_c is the mean jet centerline velocity at a given axial location, and the overbar denotes time averaging. In the Reynolds stress plot, the similarity coordinate is chosen as $r/r_{1/2}$, where r is the radial location and $r_{1/2}$ is the half-velocity radius at a given downstream location.

The Reynolds shear stress profiles at the two downstream locations in both simulations demonstrate self-similarity, consistent with experiment. However, even though the simulation with $C = 0.019$ produced a jet decay coefficient and a jet spreading rate in good agreement with experiment, we see that the Reynolds stress profiles

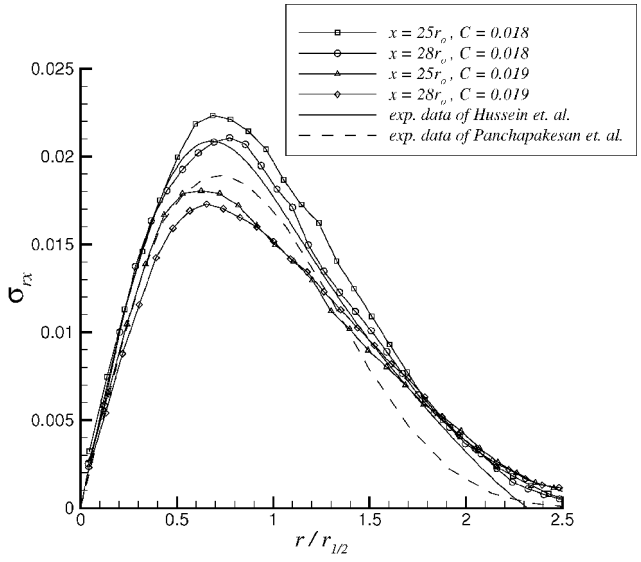

Fig. 2 Normalized Reynolds stress σ_{rx} profiles and comparison with experiments.

in the second simulation have significantly changed relative to the ones obtained in the first simulation done with $C = 0.018$. This must be due to the too dissipative nature of the Smagorinsky model. Although not shown here, similar discrepancies were observed in the other Reynolds stress components as well. The Reynolds stresses differ as much as 20% for a 5.56% change in the model constant.

We also looked at the effect of the Smagorinsky constant on transition in the shear layer. It was found that the constant did not have much influence on the level of disturbances in the shear layer. This is also evident from the fact that the jet potential core breaks up at approximately the same location in both simulations. The main finding from these simulations suggests that the value of the Smagorinsky constant has a much stronger influence on the turbulence downstream where the jet is fully turbulent.

Conclusions

Our findings in this study show some of the difficulties of using the classical Smagorinsky model as a predictive tool in turbulence simulations because the mean flow properties of our jets were found to be highly sensitive to the value of the model constants used in the computations. We believe that noise calculations will also be affected by the choice of the Smagorinsky constant. This leads us to the conclusion that one usually has no choice but to use a more robust and accurate dynamic subgrid-scale model in order to be able to do predictions using LES.

Acknowledgments

This work is sponsored by the Indiana 21st Century Research and Technology Fund. It was also partially supported by the National Computational Science Alliance under Grant CTS010032N and utilized the SGI Origin 2000 computer systems at the University of Illinois at Urbana–Champaign. Some of the computations were performed on the IBM-SP research computers of Indiana University and Purdue University.

References

[1]Freund, J. B., "Noise Sources in a Low-Reynolds-Number Turbulent Jet at Mach 0.9," *Journal of Fluid Mechanics*, Vol. 438, 2001, pp. 277–305.

[2]Bogey, C., Bailly, C., and Juvé, D., "Noise Investigation of a High Subsonic, Moderate Reynolds Number Jet Using a Compressible LES," *Theoretical and Computational Fluid Dynamics*, Vol. 16, No. 4, 2003, pp. 273–297.

[3]Constantinescu, G. S., and Lele, S. K., "Large Eddy Simulation of a Near Sonic Turbulent Jet and Its Radiated Noise," AIAA Paper 2001-0376, Jan. 2001.

[4]Zhao, W., Frankel, S. H., and Mongeau, L., "Large Eddy Simulations of Sound Radiation from Subsonic Turbulent Jets," *AIAA Journal*, Vol. 39, No. 8, 2001, pp. 1469–1477.

[5]Uzun, A., Blaisdell, G. A., and Lyrintzis, A. S., "Recent Progress Towards a Large Eddy Simulation Code for Jet Aeroacoustics," AIAA Paper 2002-2598, June 2002.

[6]Bogey, C., and Bailly, C., "Direct Computation of the Sound Radiated by a High-Reynolds-Number, Subsonic Round Jet," CEAS Workshop from CFD to CAA, Confederation of European Aerospace Societies, Nov. 2002.

[7]Smagorinsky, J. S., "General Circulation Experiments with the Primitive Equations," *Monthly Weather Review*, Vol. 91, No. 3, 1963, pp. 99–165.

[8]Germano, M., Piomelli, U., Moin, P., and Cabot, W., "A Dynamic Subgrid-Scale Eddy Viscosity Model," *Physics of Fluids A*, Vol. 3, No. 7, 1991, pp. 1760–1765.

[9]Erlebacher, G., Hussaini, M. Y., Speziale, C. G., and Zang, T. A., "Toward the Large-Eddy Simulations of Compressible Turbulent Flows," *Journal of Fluid Mechanics*, Vol. 238, 1992, pp. 155–185.

[10]Rizzetta, D. P., Visbal, M. R., and Blaisdell, G. A., "A Time-Implicit High-Order Compact Differencing and Filtering Scheme for Large-Eddy Simulation," *International Journal for Numerical Methods in Fluids*, Vol. 42, 2003, pp. 665–693.

[11]Lele, S. K., "Compact Finite Difference Schemes with Spectral-Like Resolution," *Journal of Computational Physics*, Vol. 103, No. 1, 1992, pp. 16–42.

[12]Visbal, M. R., and Gaitonde, D. V., "Very High-Order Spatially Implicit Schemes for Computational Acoustics on Curvilinear Meshes," *Journal of Computational Acoustics*, Vol. 9, No. 4, 2001, pp. 1259–1286.

[13]Bogey, C., and Bailly, C., "Three-Dimensional Non-Reflective Boundary Conditions for Acoustic Simulations: Far Field Formulation and Validation Test Cases," *Acta Acustica*, Vol. 88, No. 4, 2002, pp. 463–471.

[14]Hussein, H. J., Capp, S. C., and George, W. K., "Velocity Measurements in a High-Reynolds-Number, Momentum-Conserving, Axisymmetric, Turbulent Jet," *Journal of Fluid Mechanics*, Vol. 258, 1994, pp. 31–75.

[15]Panchapakesan, N. R., and Lumley, J. L., "Turbulence Measurements in Axisymmetric Jets of Air and Helium, Part 1. Air Jets," *Journal of Fluid Mechanics*, Vol. 246, 1993, pp. 197–223.

P. Givi
Associate Editor

Errata

Hybrid Simulation Approach for Cavity Flows: Blending, Algorithm, and Boundary Treatment Issues

R. A. Baurle and C.-J. Tam
Taitech, Inc., Beavercreek, Ohio 45430
and
J. R. Edwards and H. A. Hassan
North Carolina State University, Raleigh, North Carolina 27695

[AIAA Journal, 41(8), pp. 1463–1480 (2003)]

EQUATION (23) should read as follows:

$$P_k = \left[\mu_t\left(\frac{\partial \tilde{u}_i}{\partial x_j} + \frac{\partial \tilde{u}_j}{\partial x_i}\right) - \frac{2}{3}\delta_{ij}\left(\bar{\rho}\tilde{k} + \mu_t\frac{\partial \tilde{u}_k}{\partial x_k}\right)\right]\frac{\partial \tilde{u}_i}{\partial x_j}$$

$$\approx \mu_t\left(\frac{\partial \tilde{u}_i}{\partial x_j} + \frac{\partial \tilde{u}_j}{\partial x_i}\right)\frac{\partial \tilde{u}_i}{\partial x_j} \qquad (23)$$